Research article

Journal of RAMAN SPECTROSCOPY

Received: 1 April 2015 Revised: 28 August 2015 Accepted: 1 September 2015 Published online in Wiley Online Library: 20 October 2015

(wileyonlinelibrary.com) DOI 10.1002/jrs.4816

Raman spectra and phase composition of $MnGeO_3$ crystals

Aleksandr S. Oreshonkov,[a,b] Julia V. Gerasimova,[a] Alexandr A. Ershov,[a]* Alexander S. Krylov,[a,b] Kirill A. Shaykhutdinov,[a] Aleksandr N. Vtyurin,[a,b] Maxim S. Molokeev,[a,c] Konstantin Y. Terent'ev[a,b] and Natalia V. Mihashenok[a]

$MnGeO_3$ single-crystal samples have been synthesized by optical zonal melting and spontaneous crystallization. X-ray crystal analysis showed the first sample to be a two-phase one with phase ratio as follows: 17% – monoclinic *C*2/*c*, and 83% – orthorhombic *Pbca*; the phase ratio of the second sample was unknown. Raman spectra have been produced for these samples. Lattice dynamics has been simulated and polarization dependencies of lines' intensities have been analyzed to interpret experimental Raman spectra and to attribute lines to the spectra of monoclinic and orthorhombic phases. Copyright © 2015 John Wiley & Sons, Ltd.

Additional supporting information may be found in the online version of this article at the publisher's web site.

Keywords: Raman spectroscopy; lattice dynamics; Raman tensor analysis; orthopyroxene; clinopyroxene

Introduction

To predict crystal structures and physical properties of minerals under high pressure and temperature is among the most exciting problems of modern structural mineralogy; to solve this problem would be a gain in the knowledge of composition, structure, and evolution of the earth shells. Pyroxenes are widely occurring components of the Earth crust; they comprise about 4% of its continental mass. The main motif of the pyroxene structure is the chains of SiO_4 tetrahedra extending along *c* axis. Pyroxenes can be divided into orthorhombic (orthopyroxenes) and monoclinic (clinopyroxenes).[1,2] Intimate relationship between monoclinic and orthorhombic pyroxene is crystallographically due to simple polysynthetic twinnings and polysymmetry of the parts of elementary structural units.[3] The knowledge about regularities of the structure of silicates can be substantially expanded by investigation of germanium-containing analogs. Proceeding from simple crystallochemical principles, many germanates can be considered structural models of corresponding silicates of abyssal origin. Under high pressure, the radii of anions composing the structure reduce differently. In oxygen compounds, large O^{2-} anions are more compressible than smaller cations; therefore, the ratio of ion radii (r_{cat}/r_O) increases with pressure. Under normal pressure, the radius of Ge^{4+} is more than the radius of Si^{4+} by about 20%. So, because of initial ratio of Ge^{4+} and O^{2-}, bigger compared with the silicates, the germanates need smaller pressure for analogous phase transitions; many of them crystallize even under normal pressure in structural forms which occur in the silicates under high pressures only.[4] $MnGeO_3$ is the closest germanium-containing substitute of widely occurring pyroxene $MgSiO_3$.[5] Recently, silicates and oxide compounds have been taking up new areas of applications, driving, in some cases, metals out. For a long time, the silicate structures have been studied mostly by X-ray analysis; however, in the recent 20 years, the interest has been rising to their vibrational spectra. This is due to the development of more efficient spectrometers and methods of interpreting vibrational spectra of crystals with complex ions. This paper discusses Raman scattering applied to investigate the structure of $MnGeO_3$ germanate. Particular emphasis is given to methods of interpreting the spectra with account of crystal symmetry and polarization of Raman lines.

Experimental

Preparation of samples

$MnGeO_3$ crystal samples under study were synthesized by two methods at the Kirensky Institute of Physics (Russian Academy of Sciences, Siberian Branch).

The first single-crystal $MnGeO_3$ sample was synthesized by optical zonal melting on FZ-4000 unit (Crystal System Co, Japan). Polycrystalline $MnGeO_3$ powder was hydrostatically pressed into a rod 5 mm in diameter and 10 cm long and annealed at 1200 °C for 8 h. Then, the produced rod was placed into an optical zonal melting furnace to recrystallize. The crystal grown in the air under normal pressure at a growth rate of 1 mm/h and rotation rate of rods of 30 rpm turned into a $MnGeO_3$ single-crystal rod. However, after 2 days, the surface of the single crystal developed cracks, and in one day more, the entire single-crystal rod disintegrated into small needle-shaped fragments 1–2 mm long.

* *Correspondence to: A. A. Ershov, Kirensky Institute of Physics SB RAS, Krasnoyarsk 660036, Russia.*
E-mail: ershov@iph.krasn.ru

a *Kirensky Institute of Physics SB RAS, Krasnoyarsk 660036, Russia*

b *Siberian Federal University, Krasnoyarsk 660036, Russia*

c *Department of Physics, Far Eastern State Transport University, Khabarovsk 680021, Russia*

This behavior was also noted by Redhammer *et al.*[3] in which a single crystal of the same composition synthesized by optical zonal melting disintegrated immediately after crystallization.

The second single-crystal $MnGeO_3$ sample was synthesized by spontaneous crystallization from flux-melt. For solvent, we used $MnCl_2$ with melting temperature 615 °C.[6] Crystals were grown from flux-melt under normal pressure. Initial components of MnO amd GeO_2 in stoichiometric ratio were thoroughly mixed with solvent $MnCl_2$ and placed in specially designed alundum crucibles.[7] This device was placed into an automatically controlled furnace with silit heaters. To crystallize, the charge was heated to maximum temperature (1050 °C) to completely dissolve followed by holding for 2 h to homogenize the flux and cool it gradually at the rate of 20 °C/h. This resulted in the production of transparent brown needle-shaped single crystals extending along *c* axis. The produced crystals are shown in Fig. S1.

Powder X-ray diffraction and crystal structures

The powder X-ray diffractogram of samples synthesized by optical zonal melting (sample 1) was obtained at room temperature with D8 ADVANCE diffractometer (Bruker), VANTEC beam detector, and Cu-Kα radiation. The X-ray diffractogram was made in angular range 2θ: 5–140° with 0.016° step and point exposure time of 7.5 s. Structures and mass fraction of phases in the sample were refined by Rietveld method with TOPAS 4.2 software.[8] Refining of structure parameters was stable and yielded low *R*-factor; the basic parameters obtained are presented in Table 1. The compound crystallizes mostly in orthorhombic modification with *Pbca* space group; present is also the monoclinic *C*2/*c* modification analogous to the study of Redhammer *et al.*[3] Structures of orthorhombic and monoclinic phases of $MnGeO_3$ described in detail in Redhammer *et al.*[3] are shown in Fig. S2.

X-ray diffraction analysis of samples synthesized by spontaneous crystallization (hereinafter 2) showed them to feature pyroxene structure of orthorhombic modification with *Pbca* space group; its parameters were shown earlier in Sapronova *et al.*[7]

Table 1. Fundamental crystallographic characteristics and parameters of structure of crystal synthesized by optical zonal melting

Chemical formula	$MnGeO_3$	$MnGeO_3$
Syngony	orthorhombic	monoclinic
Space group	*Pbca*	*C*2/*c*
a, Å	19.2979(3)	9.9227(5)
b, Å	9.2448(2)	9.2794(7)
c, Å	5.4800(1)	5.2775(3)
β, °	—	101.768(5)
V, Å^3	977.65(3)	475.73 (5)
Weight fraction of phase, wt., %	83.1 (5)	16.9 (5)
Number of reflections	935	460
Number of refined parameters	102	
R_B, %	1.08	0.84
R_{wp}, %	1.72	
R_{exp}, %	0.989	
R_p, %	1.28	
χ^2	1.743	

Raman measurements

Raman measurements have been performed with triple monochromator T64000 Raman spectrometer (Horiba Jobin Yvon) operating in a double subtractive mode then detected by a charge-coupled device cooled at 140 K. The spectral resolution for the recorded Stokes-side Raman spectra was set to approximately 2 cm^{-1} (this resolution was achieved by using gratings with 1800 mm^{-1} grooves and 100 mm slits). The microRaman system based on Olympus BX41 microscope with a 50× objective lens $f = 1.2$ mm with 0.75 numerical aperture provides a focal spot diameter of about 2 μm on the sample. Single-mode argon 514.5 nm from a Stabilite 2017 (Spectra-Physics) Ar + laser of 1 mW on the sample was used as excitation light source.

To study angular dependence of intensities of Raman spectra lines on polarization direction of incident and scattered radiation, two experiment series were conducted with parallel and cross-polar polarizations of incident and scattered beams. Backscattering geometry was used. The shift of the incidence point of exciting radiation was not more than 2 μm in complete revolution by 2π.

Results and discussion

Lattice dynamics simulation

The Raman spectra produced from different points of sample 1 are shown in Fig. 1. It is apparent that spectra 2 and 3 notably differ, especially in the low-wavenumber (below 400 cm^{-1}) range, while spectrum 1 is their superposition. The full Raman spectrum of both phases can be divided into four parts: (i) <200 cm^{-1} is the range of lattice vibrations; (ii) 200–450 cm^{-1} is the range of bending vibrations; (iii) 480–580 cm^{-1} is the range of GeO_4 bridging vibrations; and (iv) 700–850 cm^{-1} is the range of ν_1 and ν_3 stretching vibrations of GeO_4 groups (denotations of internal vibration modes of GeO_4 groups are given in accordance with the study of Nakamoto[9]).

For interpretation, the Raman spectra of orthorhombic and monoclinic phases of $MnGeO_3$ were simulated within the framework of empirical lattice dynamics model with LADY software.[10]

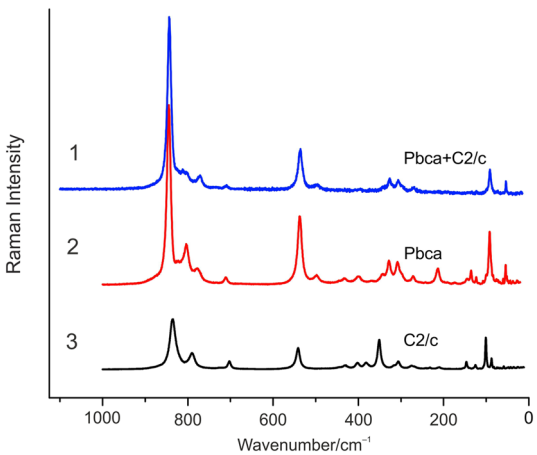

Figure 1. Three Raman spectrum types for the sample synthesized by optical zonal melting obtained from different points of its surface. Components of monoclinic C2/c, orthorhomic Pbca, and mixed phases defined by lattice dynamics simulation within the framework of semi-empirical model with LADY software.

Vibrational representation for the orthorhombic phase in the center of Brillouin zone has the following form:

$$\Gamma(Pbca) = 30A_g + 30B_{1g} + 30B_{2g} + 30B_{3g} + 30A_u + 30B_{1u} + 30B_{2u} + 30B_{3u}. \quad (1)$$

Modes active in Raman:

$$\Gamma_{\text{Raman}}(Pbca) = 30A_g + 30B_{1g} + 30B_{2g} + 30B_{3g}, \quad (2)$$

For the monoclinic phase,

$$\Gamma(C2/c) = 14A_g + 16B_g + 14A_u + 16B_u. \quad (3)$$

Modes active in Raman:

$$\Gamma_{\text{Raman}}(C2/c) = 14A_g + 16B_g. \quad (4)$$

Interatomic interactions were described with simplified Born-von Karman model.[11] This model represents a potential function as the sum of $\varphi(r)$ potentials of pair interactions of structural units, which depend on the distance between them only. This takes into consideration the stretch interactions only. Parameters of the model were refined to bring into agreement experimentally observed and calculated vibration wavenumbers. Table 2 presents comparison of experimental and calculated spectra wavenumbers for the monoclinic phase; calculation results for orthorhombic phase are presented in Table S1.

Because of the difference in the length of Ge–O bonds, normal vibrations of GeO_4 tetrahedra are distorted. Numerical simulation shows that the lines in the Raman spectra of monoclinic phase 836 and 791 cm^{-1} correspond to stretching vibrations of Ge–O, the line at 703 cm^{-1} – to distorted vibration ν_3 of GeO_4 tetrahedron. The range of 480–580 cm^{-1} corresponds to vibrations of oxygen atoms through which the tetrahedral chains are connected. In the case of monoclinic chain, the spectral band at 541 cm^{-1} corresponds to bridging (i.e., linking one tetrahedron to the other) Ge–O–Ge vibration.

Both ν_2 and ν_4 vibrations of GeO_4 tetrahedra present in range II 280–450 cm^{-1}, according to[9] for most compounds with tetrahedral ReO_4 ions $\nu_2 < \nu_4$, and intensity of ν_2 vibrations should be higher than of ν_4. Range of 200–280 cm^{-1} corresponds to mixed bending vibrations of octahedral and tetrahedral groups.

Raman spectrum of sample 2 was compared with the spectra of sample 1. On the basis of simulated lattice dynamics, the spectrum corresponds to monoclinic phase shown in Fig. S3. Raman spectra of monoclinic clinopyroxene and orthorhombic orthopyroxene phases of $MgGeO_3$ have been presented in Ross and Navrotsky;[12] structures of these phases are analogous of $MnGeO_3$. Taking in to account same symmetry and lattice structures, such main spectral parameters as number of lines and their intensities distribution for $MnGeO_3$ and $MgGeO_3$ phases should agree qualitatively – as we observed. Higher wavenumber part of Raman spectra obtained from monoclinic (*C*2/*c*) $CaMgGeO_6$ crystal[13] agrees perfectly with our higher wavenumber spectra of monoclinic $MnGeO_3$. This fact attracted special attention because the X-ray diffraction analysis of this sample corresponds to the orthorhombic phase of $MnGeO_3$.

Table 2. Comparison of calculated and experimental wavenumbers of vibrations for the monoclinic structure

№	Symm. type	ω, cm^{-1} (calc.)		ω, cm^{-1} (exp.)
1	*Bg*	839	}	836
2	*Ag*	836		
3	*Bg*	811		
4	*Ag*	790		790
5	*Ag*	703		703
6	*Bg*	664		
7	*Bg*	570	}	541
8	*Ag*	541		
9	*Ag*	442		444
10	*Bg*	438		431
11	*Bg*	383		401
12	*Ag*	381		381
13	*Ag*	353	}	351
14	*Bg*	336		
15	*Ag*	318		316
16	*Bg*	306		306
17	*Bg*	291		276
18	*Ag*	269		268
19	*Bg*	205		241
20	*Ag*	185		232
21	*Bg*	181		
22	*Ag*	176		211
23	*Bg*	140		
24	*Bg*	133		
25	*Bg*	124		
26	*Ag*	114		146
27	*Bg*	113		
28	*Ag*	110		126
29	*Ag*	80		88
30	*Bg*	67		

When interpreting the experimental spectrum within the framework of semi-empirical models, the lines have not always been unambiguously attributed to symmetry types in complex spectra. Above 300 cm^{-1}, we gained a good agreement with the number of lines and their wavenumbers, while in the low-wavenumber range, the spectral bands were observed to notably overlap – this makes unambiguous interpretation difficult.

Generally, symmetry types of vibrations are attributed by polarization measurements of spectra made on oriented samples. However, small size of samples and inhomogeneity of phase composition of sample 1 deny their orientation. Nevertheless, the lines corresponding to vibrations of different symmetry should manifest at different polarizations of incident and scattered radiation. This makes attributing symmetry of spectral lines with non-oriented samples possible by their dependencies intensities *versus* direction of radiation polarization.[14–21] This approach was used to analyze the spectrum of single-phase sample 2.

Raman tensor analysis

Spectral lines can be attributed to symmetry types for non-oriented samples by Raman tensor analysis, described in several references.[14–21]

Relative intensities of scattered light have the form

$$I \propto |e_i \mathrm{Re}_s|^2, \tag{5}$$

where e_i and e_s are unit vectors of polarization of electric field for incident and scattered light and R is the Raman tensor. For the monoclinic ($C2/c$) structure, the Raman tensors have the form

$$R_{A_g} = \begin{pmatrix} a & 0 & d \\ 0 & b & 0 \\ d & 0 & c \end{pmatrix}, R_{B_g} = \begin{pmatrix} 0 & f & 0 \\ f & 0 & e \\ 0 & e & 0 \end{pmatrix}, \tag{6}$$

Converting the Raman tensors 6 into laboratory system of coordinates and substituting them into 5, in analogy with Fukatsu

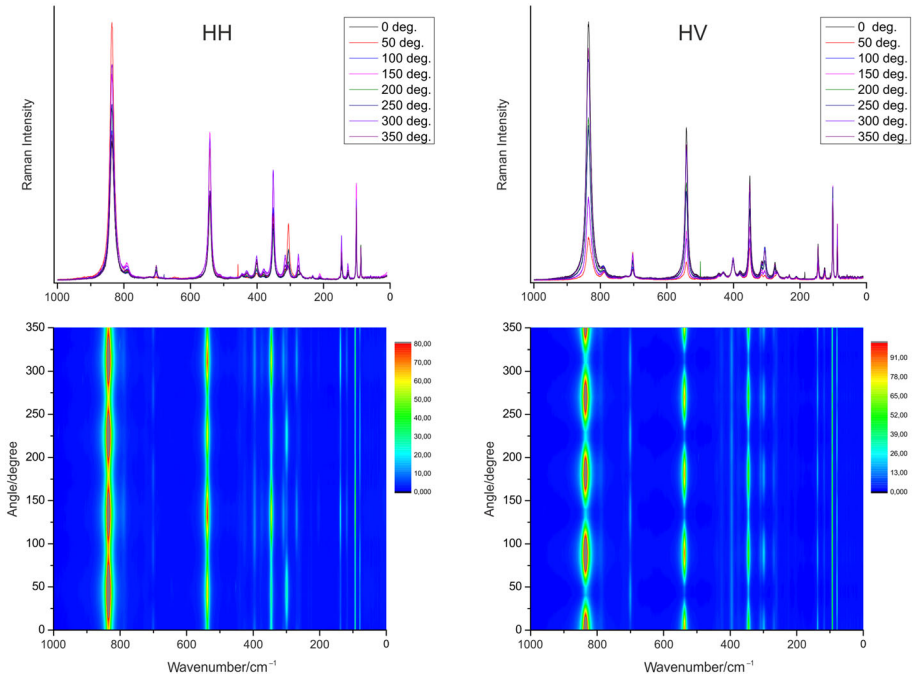

Figure 2. Dependencies of spectral intensity on polarization direction of exciting radiation. The upper figures represents the obtained Raman spectra on HH and HV polarization direction of exciting radiation and the lower ones represents the 2D graphs of Raman intensity angular dependences.

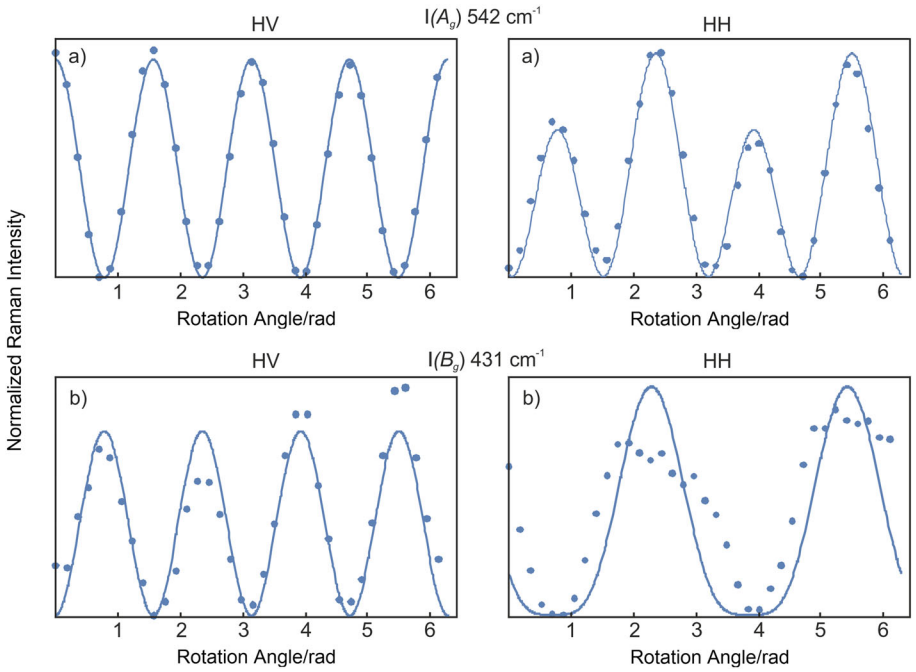

Figure 3. Angular dependencies in parallel (HH) and cross-polar (HV) polarization of incident and scattered radiation for 542 cm^{-1} and 431 cm^{-1} spectral lines, corresponding to A_g and B_g vibration modes. Solid curves are the calculation; dots are the experimental results.

et al.[15] have expressions for the dependence of spectral intensity on orientation of the sample, for parallel and cross-polar directions of polarization of exciting and scattered radiations. Angular dependencies for intensities of A_g and B_g vibration modes have the form

$$I^{||}_{A_g} \propto |\sin\theta \sin\psi[-d \sin\varphi \cos\psi + (-d \cos\theta \cos\varphi + a \sin\theta)\sin\psi] + (\cos\psi \sin\varphi + \cos\theta \cos\varphi \sin\psi)[c \sin\varphi \cos\psi + (c \cos\theta \cos\varphi - d \sin\theta)\sin\psi] + b(\cos\psi\cos\varphi + \cos\theta\sin\varphi\sin\psi)^2|^2, \quad (7)$$

$$I^{||}_{B_g} \propto |-2[f \sin\varphi \cos\psi + (f \cos\theta \cos\varphi - e \sin\theta)\sin\psi] \times (\cos\varphi \cos\psi - \cos\theta \sin\varphi \sin\psi)|^2, \quad (8)$$

$$I^{\perp}_{A_g} \propto |\sin\theta \cos\psi[d \sin\varphi \cos\psi + (d \cos\theta \cos\varphi - a \sin\theta)\sin\psi] - (\cos\theta \cos\varphi \cos\psi - \sin\varphi \cos\psi)[c \sin\varphi \cos\psi + (c \cos\theta \cos\varphi - d \sin\theta)\sin\psi] + b(\cos\theta \sin\varphi \sin\psi + \cos\varphi \sin\psi)(\cos\varphi \cos\psi - \cos\theta \sin\varphi \sin\psi)|^2, \quad (9)$$

$$I^{\perp}_{B_g} \propto |-2f\cos^2\theta \sin\varphi \cos\varphi \sin\psi \cos\psi + \cos\varphi(-e \sin\theta\cos^2\psi - 2f \sin\varphi \sin\psi \cos\psi + e \sin\theta\sin^2\psi) + \cos\theta[f\cos^2\varphi \cos(2\psi) + \sin\varphi(-f \sin\varphi\cos^2\psi + f \sin\varphi\sin^2\psi + e \sin\theta \sin(2\psi))]2 \quad (10)$$

The expressions produced are in agreement with results in Fukatsu *et al.*[15]

According to (7–10), the angular dependencies of spectral intensities (Fig. 2) for lines of different symmetry types should correspond to different pattern pairs for the parallel and crossed-polar geometries of the experiment. Classification of produced dependencies of spectral intensities by patterns yielded the following result: active in the spectrum are 14 modes of A_g type, this agrees with the selection rules for the monoclinic structure, and 5 modes of B_g type. Inconsistency by the number of B_g modes is probably due to their smaller intensity. The number of vibrational modes found by analysis of angular dependencies of the Raman tensor corresponds to the number of vibrations of the monoclinic structure. Figure 3 shows comparison of experimental and calculated dependencies in cross-polar polarizations for spectral lines at 542 cm^{-1} and 431 cm^{-1} corresponding to A_g and B_g vibration modes by lattice dynamics simulation. Figure 4 shows 3D graph of intensity of spectral line at 542 cm^{-1} *versus* angle of rotation in cross-polar polarization.

So, according to selection rules, lattice dynamics simulation and produced angular dependencies of the Raman tensor the structure of sample 2 is monoclinic.

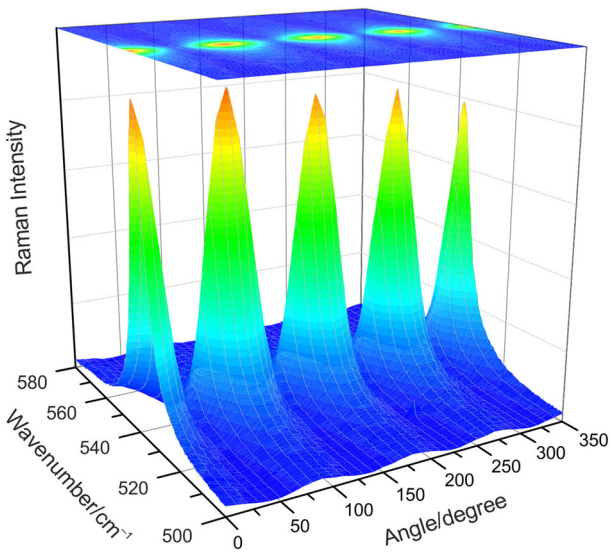

Figure 4. 3D graph of intensity of spectral line at 542 cm^{-1} *versus* angle of rotation in cross-polar polarization.

Conclusions

Raman spectra of $MnGeO_3$ synthesized by two methods optical zonal melting (sample 1) and spontaneous crystallization (sample 2) have been studied. X-ray diffraction analysis showed the first sample to contain 83% of orthorhombic and 17% of monoclinic phase. Comparison of experimental spectra to lattice dynamics simulations confirms the two-phase nature of this sample. Polarization dependencies of Raman lines' intensities for sample 2 have been obtained and symmetries of vibration modes have been found by analysis of Raman tensor. Thus, having simulated the lattice dynamics, having analyzed Raman spectrum and selection rules considered, we come to the conclusion that the structure of the second sample is monoclinic.

Acknowledgements

The work was partially supported by the RFBR through grants no. 13-02-00825.

O. A. S. and K. A. S. are partially supported by the Ministry of Science and Education of the Russian Federation.

References

[1] A. Putnis, *An Introduction to Mineral Sciences*, Cambridge University Press, Cambridge, **1992**.
[2] S. Mitra, *High-pressure Geochemistry and Mineral Physics: Basics for Planetology and Geo-material Science*, Elsevier, Amsterdam, **2004**.
[3] G. J. Redhammer, C. Volberg, G. Tippelt, *Abh. J. Mineral. Geochem.* **2012**, *189*, 103.
[4] D. Y. Pusharkovskii, *Structural Mineralogy of Silicates and their Synthetic Analogues*, Nedra, Moskow, **1986**.
[5] A. E. Ringwood, *Geochim. Cosmochim. Acta* **1991**, *55*, 2083.
[6] G. J. Redhammer, A. Senyshyn, G. Tippelt, G. Roth, *J. Phys. Condens. Matter* **2011**, *23*, 254202.
[7] N. V. Sapronova, N. V. Volkov, K. A. Sablina, G. A. Petrakovskii, O. A. Bayukov, A. M. Vorotynov, D. A. Velikanov, A. F. Bovina, A. D. Vasilyev, G. V. Bondarenko, *Phys. Status Solidi B* **2009**, *246*, 206.
[8] Bruker A. X. S., TOPAS V4.2: General Profile and Structure Analysis Software for Powder Diffraction Data, Karlsruhe, Germany, **2008**.
[9] K. Nakamoto, *Infrared and Raman Spectroscopy of Inorganic and Coordination Compounds: Applications in Coordination, Organometallics and Bioinorganic Chemistry*, John 6th Wiley and Sons, United States, **2009**.
[10] M. B. Smirnov, V. Y. Kazimirov, Lady. Software for lattice dynamics simulations. Communication of the Joint Institute for Nuclear Research, Dubna, **2001**.
[11] M. Smirnov, R. Baddour-Hadjean, *J. Chem. Phys.* **2004**, *121*, 2348.
[12] N. L. Ross, A. Navrotsky, *Am. Mineral.* **1988**, *73*, 1355.
[13] E. Lambruschi, I. Aliatis, D. Bersani, L. Mantovani, M. Tribaudino, P. P. Lottici, G. Redhammer, Abstract for 11th GeoRaman International Conference, Salzburg, Austria, **2014**, 5059.

[14] M. C. Munisso, W. Zhu, G. Pezzotti, *Phys. Status Solidi B* **2009**, *246*, 1893.
[15] K. Fukatsu, W. Zhu, G. Pezzotti, *Phys. Status Solidi B* **2010**, *247*, 278.
[16] Y. Fujii, M. Noju, T. Shimizu, H. Taniguchi, M. Itoh, I. Nishio, *Ferroelectrics* **2014**, *462*, 8.
[17] G. Pezzotti, H. Sueoka, A. A. Porporati, M. Manghnani, W. Zhu, *J. Appl. Phys.* **2011**, *110*, 013527.
[18] L. Puppulin, M. Kotaki, M. Nakamura, D. Iba, I. Moriwakic, G. Pezzotti, *J. Raman Spectrosc.* **2012**, *43*, 1957.
[19] A. Ahlawat, D. K. Mishra, V. G. Sathe, R. Kumar, T. K. Sharma, *J. Phys. Condens. Matter* **2013**, *25*, 025902.
[20] T. Sander, S. Eisermann, B. K. Meyer, P. Klar, *J. Phys. Rev. B* **2012**, *85*, 165208.
[21] M. A. Rafiq, P. Supancic, M. E. Costa, P. M. Vilarinho, M. Deluca, *Appl. Phys. Lett.* **2014**, *104*, 011902.

Supporting information

Additional supporting information may be found in the online version of this article at the publisher's web site.